CHIN. PHYS. LETT. Vol. 37, No. 10 (2020) 107505

$Fe_2Ga_2S_5$ as a 2D Antiferromagnetic Semiconductor

Chunyan Liao(廖春燕)[1], Yahui Jin(靳亚辉)[1], Wei Zhang(张薇)[2], Ziming Zhu(朱紫明)[1*], and Mingxing Chen(陈明星)[1*]

[1]*Key Laboratory of Low-Dimensional Quantum Structures and Quantum Control of Ministry of Education, Department of Physics and Synergetic Innovation Center for Quantum Effects and Applications, Hunan Normal University, Changsha 410081, China*

[2]*Fujian Provincial Key Laboratory of Quantum Manipulation and New Energy Materials, College of Physics and Energy, Fujian Normal University, Fuzhou 350117, China*

(Received 16 July 2020; accepted 7 September 2020; published online 29 September 2020)

We theoretically investigate physical properties of two-dimensional (2D) $Fe_2Ga_2S_5$ by employing first-principles calculations. It is found that it is an antiferromagnet with zigzag magnetic configuration orienting in the in-plane direction, with Néel temperatures around 160 K. The band structure of the ground state shows that it is a semiconductor with the indirect band gap of about 0.9 eV, which could be effectively tuned by the lattice strain. We predict that the carrier transport is highly anisotropic, with the electron mobility up to the order of $\sim 10^3\ \mathrm{cm}^2/(\mathrm{V\cdot s})$ much higher than the hole. These fantastic electronic properties make 2D $Fe_2Ga_2S_5$ a promising candidate for the future spintronics.

PACS: 75.50.Ee, 73.20.−r, 31.15.A−, 72.20.Jv DOI: 10.1088/0256-307X/37/10/107505

Since the successful exfoliation of graphene from graphite, two-dimensional (2D) magnetic materials have drawn a great deal of attention because they not only host the fundamental significance of the underlying physics in reduced dimensions but also show promising applications in nano-spintronics, quantum computing and on-chip optical communication.[1] Generally, the intrinsic long-range magnetic order in the spin-rotation 2D system is strongly suppressed by the enhanced fluctuations revealed by the Mermin–Wagner theorem.[2] It has not been overcome until the 2D magnetic crystals have been discovered experimentally,[3,4] where magnetic anisotropy plays a crucial role in stabilizing long-range magnetic order. For instance, 2D ferromagnetisms (FM) has been demonstrated in the monolayer CrI_3[3] and $Cr_2Ge_2Te_6$[4] via the mechanic exfoliation method. Following the discoveries mentioned above, many other magnetic layered crystals exhibit the long-range ferromagnetic order in the fewer layers, such as Fe_3GeTe_2,[5−7] VSe_2,[8] $MnSe_x$,[9] and MnSn.[10] However, the Curie temperatures observed for them are rather low (e.g., 45 K for CrI_3 and 61 K for $Cr_2Ge_2Te_6$), which limit their usage for practical applications.

On the other hand, the known intrinsic 2D antiferromagnetism (AFM) is limited to only a few candidates. One notable example is $FePS_3$,[11,12] which exhibits the relatively low Néel temperature (∼118 K). In contrast to the 2D FM, the main advantages of 2D antiferromagnetic materials are the robustness against perturbation due to magnetic fields, no stray fields, ultrafast dynamics and the capability to produce large magnetotransport effects.[13−15] Moreover, 2D AFM provides an excellent platform to tune the magnetic structures by lattice strain[16] and has a faster switching between difference magnetic states over FM.[17] Hence, it is highly desirable to identify 2D antiferromagnetic materials with robust ground state, high carrier mobility and higher Néel temperature.

In this work, we systematically investigate physical properties of 2D $Fe_2Ga_2S_5$, in which the bulk form is van der Waals layered crystal synthesized over forty years ago.[18] Based on first-principles calculations, we predict that 2D $Fe_2Ga_2S_5$ is a dynamically stable magnetic semiconductor with the zigzag-type antiferromagnetic structure favoring in-plane direction. The Néel temperature is evaluated using Monte Carlo simulations, which reaches up to about 160 K. In the ground state, 2D $Fe_2Ga_2S_5$ belongs to the indirect band gap semiconductor (∼0.9 eV). We find that the electron and hole exhibit distinct transport properties. The effective mass of the electrons is small, whereas it is much larger for the holes, especially along the y direction. As a result, the electrons have fairly high mobility, which reaches the order of $\sim 10^3\ \mathrm{cm}^2/(\mathrm{V\cdot s})$. Finally, we investigate that the electronic structure can be effectively tuned by bi-axial strains. Our work reveals an existing 2D AFM material with a robust magnetic structure and high mobility, which could be useful in the nanoscale devices based on 2D AFM spintronics.

Supported by the National Natural Science Foundation of China (Grant Nos. 11704117, 11774084, U19A2090 and 11974076), and the Project of Educational Commission of Hunan Province of China (Grant No. 18A003).

*Corresponding authors. Email: zimingzhu@hunnu.edu.cn; mxchen@hunnu.edu.cn

© 2020 Chinese Physical Society and IOP Publishing Ltd

Computational Method. Our first-principles calculations were performed on the basis of the density functional theory, using a plane-wave basis set and projector augmented wave method,[19] as implemented in the Vienna *ab initio* simulation package (VASP).[20,21] The generalized gradient approximation (GGA) parameterized by Perdew, Burke, and Ernzerhof (PBE) was adopted for the exchange-correlation functional. The energy cutoff was set to 360 eV, and a 11×11 Monkhorst–Pack k mesh was used for the Brillouin zone (BZ) sampling. The lattice constants and the atomic positions were fully optimized until the residual forces were less than 10^{-3} eV/Å. The convergence criterion for the total energy was set to be 10^{-6} eV. Thickness of the vacuum layer for the slab model was 16 Å to avoid the interaction between the periodically repeated images. To account for the correlation effects on the transition metal Fe, the GGA+U method with $U = 4$ eV for Fe-3d orbital was adopted.[22]

The dynamic stability of monolayer is investigated by phonon spectrum using a finite difference method as implemented the PHONONPY code.[23] The magnetic transition temperatures were estimated by Monte Carlo simulations using the VAMPIRE package.[24] In the simulation, a supercell with size 15×15 was used.

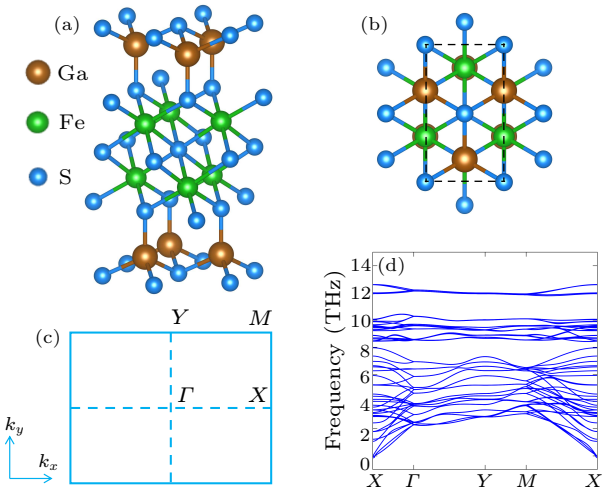

Fig. 1. (a) Perspective view and (b) top view of the 2D $Fe_2Ga_2S_5$ structure. The magnetic unit cell contains two unit cells (the dashed box). (c) Two-dimensional Brillioun zone (BZ) associated with the magnetic unit cell, where high-symmetry points are labelled. (d) Phonon dispersion of 2D $Fe_2Ga_2S_5$ along the high symmetry line.

Crystal and Magnetic Structure. The bulk $Fe_2Ga_2S_5$ is a van der Waals layered crystal, obtained by the chemical vapor transport using iodine.[18] This compound in the 3D case shares the trigonal crystal with space group $R\bar{3}m$ (No. 166), while its 2D phase, i.e., the monolayer, is lowered to the space group of $P\bar{3}m1$ (No. 164) with nine atoms in a primitive unit cell. The perspective view in Fig. 1(a) shows that the monolayer $Fe_2Ga_2S_5$ contains two Fe and Ga layers, which are sandwiched by five S layers alternatively. Figure 1(b) shows that a bipartite honeycomb lattice is formed by two Fe triangular lattices, which are linked together by S. It should be mentioned that the intralayer Fe–S–Fe bonds play a crucial role in stabilizing the long-range magnetic order, leading to AFM magnetic configurations.[25,26] The optimized lattice constant is given in Table 1. To check its dynamical stability, we calculate the phonon dispersion along the high-symmetry lines as shown in Fig. 1(d). Note that the symmetry of the BZ [see Fig. 1(c)] belongs to $C2/m$ space group due to the requirement of zigzag-type antiferromagnetic configuration determined below. One can see that there is no soft mode appearing in the phonon spectrum, indicating that the monolayer $Fe_2Ga_2S_5$ is dynamically stable.

Table 1. Calculated lattice constants a (in units of Å), magnetic moment μ per Fe ion (in μ_B), the total free energy per formula unit (in meV) for the distinct magnetic structures. Here, the magnetic configuration in the ground state is taken as the reference (with its energy set as zero).

a	μ	$E^x_{\rm FM}$	$E^x_{\rm Neel}$	$E^x_{\rm Stripy}$	$E^x_{\rm zigzag}$
3.701	3.46	206.982	1131.899	1247.404	0

Usually the compounds with transition metal element will exhibit magnetic properties. The magnetism of the 2D $Fe_2Ga_2S_5$ is mainly from Fe. The Fe ions own the nominal valence of +2, in which there has six electrons in the d shell. One can observe that each Fe ion lies in the center of an octahedron formed by the nearby six S ions. The crystal field in an octahedron splits the five-fold degenerate 3d orbit in the Fe ions into the e_g and t_{2g} orbitals, with e_g higher in energy. The spin configuration in Fe^{2+} takes the form of $(t^4_{2g}e^2_g)$ since there exists six d electrons, resulting in the high spin state of $S = 2$ for a single Fe^{2+}. The spin magnitude is consistent with the magnetic moment of $\sim 3.5\mu_B$, as listed in Table 1.

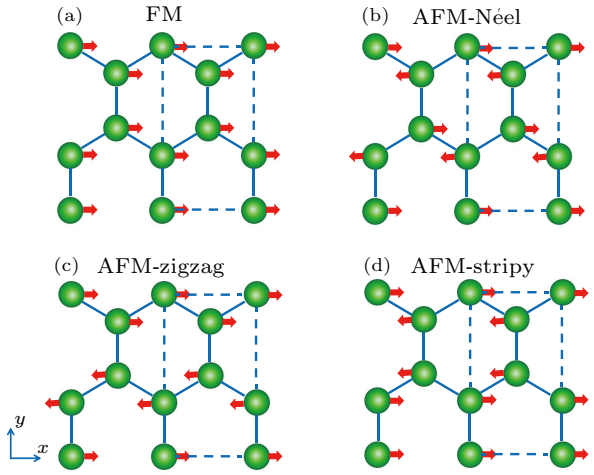

Fig. 2. Four considered magnetic configurations: (a) FM, (b) AFM-Néel, (c) AFM-zigzag, and (d) AFM-stripy. Here the nonmagnetic atoms are not shown.

Nakatsuji *et al.*[25] have determined that the quasi-2D $Fe_2Ga_2S_5$ can exhibit the long-range AFM coupling through the observations of magnetic specific heat. In order to verify the magnetic configuration in the ground state of 2D $Fe_2Ga_2S_5$, we need to compare the energies for four typical types of magnetic configurations, including FM, AF-Néel, AF-zigzag and AF-stripy as illustrated in Fig. 2. Here the spin-orbit coupling has been included for the energy calculation of each magnetic structure, and the magnetic easy axis is determined to prefer the x direction. As listed in Table 1, the ground state in 2D $Fe_2Ga_2S_5$ displays the AFM-zigzag ordering with the orientation along x.

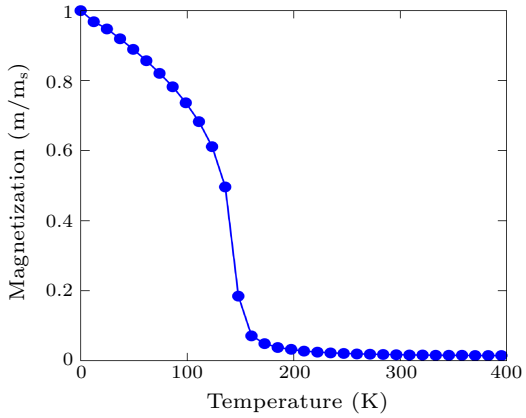

Fig. 3. The normalized magnetic moment of $Fe_2Ga_2S_5$ monolayer as a function of temperature by Monte Carlo simulations.

To better understand the magnetic structure, we consider the following classical Heisenberg-like spin model[24] on a honeycomb lattice:

$$H = -\sum_{i,j} J_{ij} \boldsymbol{S}^i \cdot \boldsymbol{S}^j - K \sum_i (S_z^i)^2, \qquad (1)$$

where the spin vectors are normalized, i and j represent the Fe sites, J_{ij} means the exchange coupling strength between sites i and j, and K labels the magnetic anisotropy strength. In the exchange term, we include the first-, second- and third-neighboring exchange integrals, respectively. The values of the parameters J_{ij} and K are extracted from the DFT calculations. In order to calculate K, the hard direction of magnetization is chosen to be the z-axis since the ground state energy increase per formula unit along z ($\sim$4.202 meV) is larger than that along y ($\sim$0.973 meV). The results show that the magnetic interaction for the first neighboring ions between two Fe is FM coupling ($J_1 > 0$), while it is AFM coupling for the second- and third neighboring ions ($J_2 < 0$ and $J_3 < 0$) (see Table 2). This can be understood according to the Goodenough–Kanamori–Anderson rules.[27–30] All the magnetic couplings in 2D $Fe_2Ga_2S_5$ originate from the superexchange interaction mediated by the S ion. The angle of Fe–S–Fe bonds for J_1, J_2 and J_3 are 88.49°, 101.18° and 180°, respectively. Generally, superexchange with 90° favors the FM coupling between two magnetic sites with partially occupied d shells, while that with 180° prefers the AFM coupling. As the angle changes from 90° to 180°, the magnetic coupling presents the competition between AFM and FM. Here J_2 and J_3 could be regarded as super-exchange interaction, and J_3 is much greater than J_2. This may be because the hybridization among Fe(d)-S(p)-Fe(d) is stronger for J_3 interactions as mentioned in Ref. [16]. Furthermore, we estimate the magnetic transition temperature by performing Monte Carlo simulations. One can see that the Néel temperature is around 160 K as depicted in Fig. 3, which agrees with the experimental evidence.[25] It should be mentioned that for the double and three layers, the intralayer magnetic ordering is still AFM-zigzag along in-plane direction, while the interlayer magnetic coupling is FM.

Table 2. The parameters used in the spin model (1) (in meV), and the estimated Néel temperature T_N (in K). Here, J_1, J_2 and J_3 are the first, second and third neighbor exchange coupling strength, respectively.

J_1	J_2	J_3	K	T_N
71.103	−1.496	−45.862	4.202	161

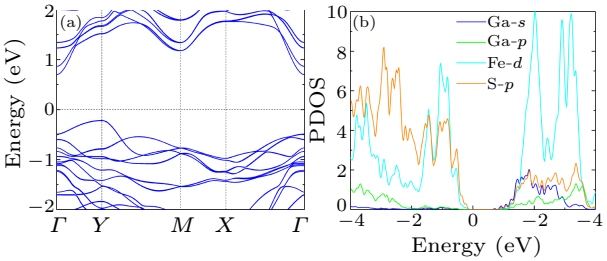

Fig. 4. (a) Calculated band structures and (b) orbital projected density of states (PDOS) for 2D $Fe_2Ga_2S_5$. SOC is included in the calculations.

Electronic Property and Mobility. After fixing the ground state, we now turn to discuss the electronic structure of 2D $Fe_2Ga_2S_5$. In Fig. 4(a), we plot the band structure with SOC included, revealing that it is a semiconducting electronic state with indirect band gap of around 0.9 eV. The conduction band minimum (CBM) is located at the Γ point and the valence band maximum (VBM) is situated at the Y point. The calculated projected density of states in Fig. 4(b) show that the low-energy bands are mainly dominated by Fe-d and S-p orbitals. In addition, the bands at the general moment points are doubly degenerate owing to the appearance of the combined $\mathcal{PT}$ symmetry. This feature confirms that the J_3 interactions belong to AFM couplings.

One may notice that there is a substantial difference for the band dispersion between CBM and VBM. The bands surrounding CBM feature the relatively strong dispersion, while the dispersion around VBM is much suppressed, especially for the Y–Γ direction. To clarify the difference, we calculate the ef-

fective masses along x and y, as listed in Table 3. We find that the effective mass of electron is smaller than that of hole along x and y directions. In particular, $m_y^{\mathrm{h}*} = 2.346m_0$ (m_0 is free electron mass), which is over 12 times larger than $m_y^{\mathrm{e}*} = 0.198m_0$. In addition, the hole effective mass in the y axis is about seven times of that in the x axis. By contrast, the electron effective mass for the two directions almost remains unchanged.

Table 3. Calculated effective masses and carrier mobilities for 2D $Fe_2Ga_2S_5$. Here m_0 is the free electron mass. The mobilities are evaluated at 300 K, shown in units of $10^3\,\mathrm{cm}^2/(\mathrm{V{\cdot}s})$.

Carrier type	m_x^*/m_0	m_y^*/m_0	$\mu_x^{2\mathrm{D}}$	$\mu_y^{2\mathrm{D}}$
e	0.196	0.198	1.876	1.836
h	0.349	2.346	0.592	0.0139

The difference can be explained by comparing the charge distributions. Here we show the charge distributions of 2D $Fe_2Ga_2S_5$ for the two states at CBM and VBM, as plotted in Fig. 5. Remarkably, the charge distribution at the VBM state is confined in the y direction, while they are mostly extended for the CBM state along x direction as well as the CBM state along both the directions. These results are consistent with the variation behavior of band dispersions around CBM and VBM.

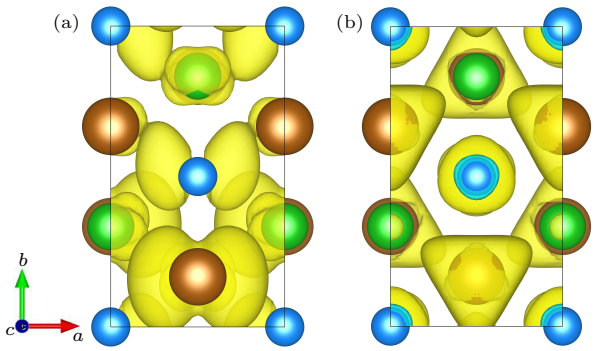

Fig. 5. Charge distribution (side view of the unit cell) for (a) VBM state and (b) CBM state of 2D $Fe_2Ga_2S_5$ using the isosurface value of 0.000512 eV/Å^3.

To further capture the distinct band dispersions between VBM and CBM, we proceed to the properties of the carrier transport along x and y directions. Based on the deformation potential theory, the carrier mobilities in 2D can be evaluated by the following formula:[31,32]

$$\mu_i^{2\mathrm{D}} = \frac{e\hbar^3 C_i^{2\mathrm{D}}}{k_{\mathrm{B}} T m_d^* m_i^* (\mathcal{D}_i)^2}, \tag{2}$$

where $C_i^{2\mathrm{D}} = (1/S_0)(\partial^2 E_{\mathrm{S}}/\partial\varepsilon_i^2)$ is the 2D elastic constant, E_{S} and V_0 are the energy and the volume of the system, $\varepsilon_i = (\ell_i - \ell_i^0)/\ell_i^0$ means the strain along the i direction, $m_d^* = (m_x^* m_y^*)^{1/2}$ is the average effective mass, and $\mathcal{D}_i = \partial\Delta/\partial\varepsilon_i$ represents the deformation potential constant, with Δ the shift of the band edge energy under strain. The predicted carrier mobilities of 2D $Fe_2Ga_2S_5$ at $T = 300$ K are highly anisotropic as listed Table 3. The mobilities for electron reach the order of $10^3\,\mathrm{cm}^2/(\mathrm{V{\cdot}s})$ at room temperature. In contrast, the hole mobilities are much lower. For instance, the hole mobility along the y axis is about 130 times lower than the electron mobility. Although the value of the electron mobility is lower than that of graphene [$\sim$120000 $\mathrm{cm}^2/(\mathrm{V{\cdot}s})$ at 240 K],[33] it is comparable to that of phosphorene [$10^3\,\mathrm{cm}^2/(\mathrm{V{\cdot}s})$ at 300 K][34] and much higher than that of 2D MoS_2 [$\sim$200 $\mathrm{cm}^2/(\mathrm{V{\cdot}s})$ at room temperature].[35] Moreover, the high electron mobility and the asymmetry of transport performance between hole and electron render 2D $Fe_2Ga_2S_5$ a very promising potential in the AFM spintronics.

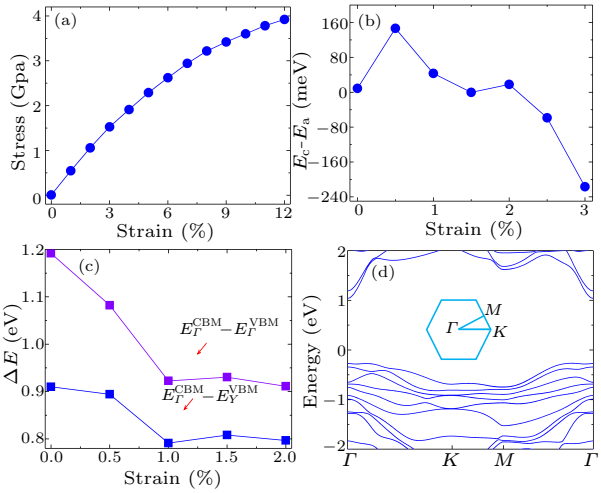

Fig. 6. (a) Calculated strain and stress relation for 2D $Fe_2Ga_2S_5$. The effect of strain on (b) energy difference of zigzag AFM state with the orientations along x and z, as well as (c) energy difference between CBM and VBM for different high symmetry points. (d) The band structure of 2D $Fe_2Ga_2S_5$ for paramagnetic phase.

Interestingly, we explore the effect of biaxial strain on the magnetic configurations and electronic structures. It is well known that 2D materials have the advantage to sustaining the large strain, opening the possibility to tune its physical properties. In Fig. 6(a), we shows the strain-stress relation obtained by DFT calculations. We find that the strain value in the linear elastic regime is up to $\sim$5%, and the critical strain is about $\sim$12%. Figure 6(b) demonstrates that the preferred orientation of zigzag AFM is tuned from x to z as the biaxial strain is increased up to 2%. Furthermore, we plot the variation of energy difference for the Γ point as well as the Γ and Y points toward the biaxial strain, as shown in Fig. 6(c). One can see that the band gap drops from 0.9 eV to 0.8 eV with varying strain from zero to 1% and almost remains unchanged with increasing up to 2%. Here we should emphasize that fundamental band gap remains indirect with strain up to 2%. Lastly, we calculated the band structure for 2D paramagnetic $Fe_2Ga_2S_5$ as plot-

ted in Fig. 6(d), indicating that it is a semiconducting state with direct band gap of about 1.15 eV.

Bulk Magnetic Order and Electronic Properties. So far we have only studied the ground state of 2D $Fe_2Ga_2S_5$, which is determined to be in-plane AFM-zizgag. It is important to further consider the detailed magnetic structure for 3D $Fe_2Ga_2S_5$, although it has already been reported to be AFM.[25] We find that for the bulk $Fe_2Ga_2S_5$, the intralayer magnetic ordering is still AFM-zigzag orienting along the x axis, whereas the interlayer magnetic ordering is FM coupling as listed in Table 4. The Néel temperature is estimated to be 176 K, close to the 2D case. Figure 7 shows that 3D $Fe_2Ga_2S_5$ is an indirect band gap semiconductor ($\sim$0.42 eV), with electron and hole located at Γ and Y, respectively. One can see that the in-plane dispersions for both electron and hole in 3D $Fe_2Ga_2S_5$ are similar to those of 2D $Fe_2Ga_2S_5$, and the out-of-plane dispersion for electron is far stronger than that of hole as listed in Table 5. We further evaluate the 3D carrier mobilities based on the deformation theory,[31,32] showing that the mobility for the electron is higher than that for the hole. For example, the electron mobility in the in-plane direction reaches up to the order of 10^2 cm^2/(V·s) at room temperature, which is much higher than that of hole. In addition, the 3D carrier mobilities for both electron and hole are lower as compared to those for 2D $Fe_2Ga_2S_5$.

Table 4. The parameters used in the spin model (1) (in meV) for 3D $Fe_2Ga_2S_5$, and the estimated Néel temperature T_N (in K). J_4 is the interlayer first neighbor exchange coupling strength.

J_1	J_2	J_3	J_4	K	T_N
74.315	−5.746	−35.127	0.749	7.125	176

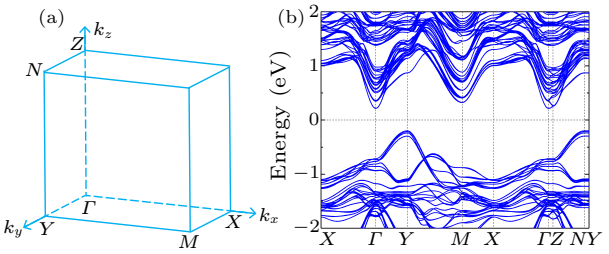

Fig. 7. (a) BZ of the magnetic unit cell and (b) the corresponding band structures for 3D $Fe_2Ga_2S_5$.

Table 5. Calculated effective masses and carrier mobilities for 3D $Fe_2Ga_2S_5$. The mobilities are evaluated at 300 K and are shown in units of 10^3 cm^2/(V·s).

Carrier type	m_x^*/m_0	m_y^*/m_0	m_z^*/m_0	μ_x^{3D}	μ_y^{3D}	μ_z^{3D}
e	0.203	0.206	0.403	0.151	0.149	0.076
h	0.383	1.055	453.516	1.4×10^{-3}	4.9×10^{-4}	1.1×10^{-6}

In summary, we have systemically investigated the physical properties of 2D $Fe_2Ga_2S_5$, and revealed that it is an AFM semiconductor with indirect band gap of around 0.9 eV. We predict that the ground state has the AFM ordering orienting along x direction and the Néel temperature is estimated to be about 160 K using Monte Carlo simulations. Furthermore, we find that it has the fairly high electron mobility, which is up to the order of $\sim 10^3$ cm^2/(V·s). By contrast, the hole mobility is much lower than the electron mobility, especially in the y direction. The highly anisotropy of carrier mobilities provides the channel to effectively control the transport properties via doping.

We thank Si Li, Yalong Jiao, Bo Tai, Jun Hu and Shengyuan A. Yang for valuable discussions. Also, we acknowledge computational support from Texas Advanced Computing Center and H2 clusters in Xi'an Jiaotong University.

References

[1] Gong C and Zhang X 2019 *Science* **363** eaav4450
[2] Mermin N D and Wagner H 1966 *Phys. Rev. Lett.* **17** 1133
[3] Huang B, Clark G, Navarro-Moratalla E, Klein D R, Cheng R, Seyler K L, Zhong D, Schmidgall E, McGuire M A, Cobden D H *et al.* 2017 *Nature* **546** 270
[4] Gong C, Li L, Li Z, Ji H, Stern A, Xia Y, Cao T, Bao W *et al.* 2017 *Nature* **546** 265
[5] Zhu J X, Janoschek M, Chaves D S, Cezar J C, Durakiewicz T, Ronning F, Sassa Y, Mansson M, Scott B L, Wakeham N, Bauer E D and Thompson J D 2016 *Phys. Rev. B* **93** 144404
[6] Zhuang H L, Kent P R C and Hennig R G 2016 *Phys. Rev. B* **93** 134407
[7] Deng Y, Yu Y, Song Y, Zhang J, Wang N Z, Sun Z, Yi Y, Wu Y Z *et al.* 2018 *Nature* **563** 94
[8] Bonilla M, Kolekar S, Ma Y, Diaz H C, Kalappattil V, Das R, Eggers T, Gutierrez H R, Phan M H and Batzill M 2018 *Nat. Nanotechnol.* **13** 289
[9] O'Hara D J, Zhu T, Trout A H, Ahmed A S, Luo Y K, Lee C H, Brenner M R, Rajan S, Gupta J A, McComb D W *et al.* 2018 *Nano Lett.* **18** 3125
[10] Yuan Q Q, Guo Z, Shi Z Q, Zhao H, Jia Z Y, Wang Q, Sun J, Wu D and Li S C 2020 *Chin. Phys. Lett.* **37** 077502
[11] Lee J U, Lee S, Ryoo J H, Kang S, Kim T Y, Kim P, Park C H, Park J G and Cheong H 2016 *Nano Lett.* **16** 7433
[12] Wang X, Du K, Liu Y Y F, Hu P, Zhang J, Zhang Q, Owen M H S, Lu X, Gan C K, Sengupta P *et al.* 2016 *2D Mater.* **3** 031009
[13] Jungwirth T, Marti X, Wadley P and Wunderlich J 2016 *Nat. Nanotechnol.* **11** 231
[14] Baltz V, Manchon A, Tsoi M, Moriyama T, Ono T and Tserkovnyak Y 2018 *Rev. Mod. Phys.* **90** 015005
[15] Gong W, Leung C H, Sin C K, Zhang J, Zhang X, Xi B and Zhu J 2020 *Chin. Phys. Lett.* **37** 027501
[16] Sivadas N, Daniels M W, Swendsen R H, Okamoto S and Xiao D 2015 *Phys. Rev. B* **91** 235425
[17] Meiklejohn W H and Bean C P 1957 *Phys. Rev.* **105** 904
[18] Dogguy-Smiri L and Dung N H 1982 *Acta Crystallogr. B* **38** 372
[19] Blöchl P E 1994 *Phys. Rev. B* **50** 17953
[20] Kresse G and Furthmüller J 1996 *Phys. Rev. B* **54** 11169
[21] Kresse G and Joubert D 1999 *Phys. Rev. B* **59** 1758
[22] Grau-Crespo R, Corà F, Sokol A A, de Leeuw N H and

Catlow C R A 2006 *Phys. Rev. B* **73** 035116
[23] Togo A, Oba F and Tanaka I 2008 *Phys. Rev. B* **78** 134106
[24] Evans R F L, Fan W J, Chureemart P, Ostler T A, Ellis M O A and Chantrell R W 2014 *J. Phys.: Condens. Matter* **26** 103202
[25] Nakatsuji S, Tonomura H, Onuma K, Nambu Y, Sakai O, Maeno Y, Macaluso R T and Chan J Y 2007 *Phys. Rev. Lett.* **99** 157203
[26] Reja S, Anisimov P S and Daghofer M 2017 *Phys. Rev. B* **96** 085144
[27] Anderson P W 1950 *Phys. Rev.* **79** 350
[28] Goodenough J B 1955 *Phys. Rev.* **100** 564
[29] Goodenough J B 1958 *J. Phys. Chem. Solids* **6** 287
[30] Kanamori J 1959 *J. Phys. Chem. Solids* **10** 87
[31] Bardeen J and Shockley W 1950 *Phys. Rev.* **80** 72
[32] Xi J, Long M, Tang L, Wang D and Shuai Z 2012 *Nanoscale* **4** 4348
[33] Bolotin K I, Sikes K J, Hone J, Stormer H L and Kim P 2008 *Phys. Rev. Lett.* **101** 096802
[34] Li L, Yu Y, Ye G J, Ge Q, Ou X, Wu H, Feng D, Chen X H and Zhang Y 2014 *Nat. Nanotechnol.* **9** 372
[35] Radisavljevic B, Radenovic A, Brivio J, Giacometti V and Kis A 2011 *Nat. Nanotechnol.* **6** 147